



## OPEN The antidiabetic effect of safflower yellow by regulating the GOAT/ghrelin/GHS-R1a/cAMP/TRPM2 pathway

Yunxiao Ma, Haifeng Zhang, Qihui Yan, Ping Wang, Weiying Guo<sup>✉</sup> & Lu Yu<sup>✉</sup>

Safflower yellow (SY), derived from *Carthamus tinctorius* L., is a valuable natural edible pigment that exhibits anti-type 2 diabetes mellitus (T2DM) efficacy; however, its mechanism of action is unclear, which hinders its effective use. In this study, we examined the impact of SY on glucose metabolism and insulin secretion both in vivo and in vitro and elucidated the possible underlying mechanism. First, molecular docking demonstrated a strong binding affinity between SY and ghrelin *O*-acyltransferase (GOAT) protein, which was validated by a cell heat transfer assay (CETSA) and drug affinity response target stability (DARTS) in MIN6 cells. In MIN6 cells, SY increased insulin secretion and showed time- and dose-dependent inhibition of GOAT expression and acyl ghrelin (AG) secretion without affecting the overall levels of ghrelin. Furthermore, ELISA revealed that SY enhanced high glucose (HG)-induced insulin secretion, and immunofluorescence revealed the co-localization of GOAT and ghrelin in MIN6 cells, which was suppressed by SY treatment. The mechanism analysis by Western blot demonstrated that SY downregulated the protein levels of GOAT and GHS-R1a in MIN6 cells while increasing HG-stimulated cAMP and activation of transient receptor potential melastatin 2 (TRPM2). In in vivo experiments, the intraperitoneal injection of SY significantly improved pathological damage to the pancreas, glucose tolerance, and insulin resistance in a mouse model of high-fat diet (HFD)/streptozotocin (STZ)-induced T2DM in a dose-dependent manner. SY enhanced insulin secretion by inhibiting the GOAT/ghrelin system in vivo. In conclusion, we demonstrated that SY exhibits an observable protective effect on diabetes through the GOAT/ghrelin/GHS-R1a/cAMP/TRPM2 pathway. Our findings provide a basis for further investigation of the hypoglycemic mechanism of SY and its potential for further development and utilization.

**Keywords** Safflower yellow, GOAT, Ghrelin, GHS-R1a, T2DM

### Abbreviations

SY	Safflower yellow
T2DM	Type 2 diabetes mellitus
GOAT	Ghrelin <i>O</i> -acyltransferase
CETSA	Cellular thermal shift assay
DARTS	Drug affinity responsive target stability
AG	Acyl ghrelin
TRPM2	Transient receptor potential melastatin 2
HFD	High fat diet
STZ	Streptozotocin
HG	High glucose
CHM	Chinese herbal medicine
HSYA	Hydroxysafflor yellow A
DAG	Des-acyl ghrelin
GHS-R1a	Growth hormone secretagogue receptor

Department of Endocrinology, Interventional Therapy, and Otolaryngology-Head and Neck Surgery of First Hospital of Jilin University, State Key Laboratory for Diagnosis and Treatment of Severe Zoonotic Infectious Diseases, Key Laboratory for Zoonosis Research, Ministry of Education, Institute of Zoonosis, College of Veterinary Medicine, Jilin University, Changchun 130000, China. ✉email: guowuy@jlu.edu.cn; yu\_lu@jlu.edu.cn

GSIS	Glucose-stimulated insulin secretion
VGCC	Voltage-gated $\text{Ca}^{2+}$ channel
cAMP	Cyclic adenosine monophosphate
DMSO	Dimethyl sulfoxide
FBG	Fasting blood glucose
OGTT	Oral glucose tolerance test
ITT	Insulin tolerance test
AUC	Area under the curve
DPP	Dipeptidyl peptidase
EPAC	Exchange protein directly activated by cAMP

Diabetes mellitus, particularly type 2 diabetes mellitus (T2DM), is a serious global health concern. Despite the availability of a diverse array of therapeutic substances for diabetes management, several challenges remain to be overcome<sup>1</sup>. As an alternative to modern medicine, Chinese herbal medicine (CHM) has proven effective against diabetes. Although CHM cannot fully substitute traditional pharmacotherapy, it offers the potential to decrease medication dosages or minimize the quantity of drugs employed for glucose regulation<sup>2</sup>. Safflower yellow (SY) is the primary component of *Carthamus tinctorius* L. and has been widely used in China for the treatment of cardiovascular, cerebrovascular, and gynecological diseases<sup>3</sup>. Accumulating evidences have demonstrated that SY treatment significantly reduces fat mass, enhances glucose homeostasis, and ameliorates insulin resistance in high-fat diet (HFD)-induced obese mice<sup>4–6</sup>. Despite extensive research, the mechanism through which SY prevents diabetes remains unclear. Therefore, we sought to further investigate the therapeutic properties of SY in diabetes and elucidate its underlying molecular mechanism.

Ghrelin, a peptide consisting of 28-amino, is primarily produced by the X/A-like cells in the gastrointestinal tract, and ghrelin mainly exists in two forms: des-acyl ghrelin (DAG) and acyl ghrelin (AG)<sup>7</sup>. Ghrelin was initially discovered as a natural ligand of the growth hormone secretagogue receptor (GHS-R1a), which promotes the production of growth hormones<sup>7,8</sup>. Unlike DAG, AG undergoes acylation of its third amino acid (serine 3) by ghrelin O-acyltransferase (GOAT)<sup>9</sup>. The acylation process is necessary for binding to GHS-R1a, which stimulates its hormone-releasing properties.

The original purpose of ghrelin is to promote appetite; however, it has a variety of peripheral and central functions such as regulating body weight, glucose homeostasis, fat distribution, reward-seeking behavior, learning, and memory<sup>10,11</sup>. According to numerous studies, AG inhibits glucose-stimulated insulin secretion (GSIS) in isolated islets and pancreatic  $\beta$ -cells<sup>12,13</sup>. Furthermore, research has demonstrated that removing the genes responsible for ghrelin (Ghrl) and GOAT (Mboat4) improves glucose tolerance and increases insulin secretion in mice that had been fasted for 16 h<sup>14,15</sup>. Consequently, blocking the GOAT/ghrelin/GHS-R1a pathway is a promising approach for the treatment of diabetes.

Transient receptor potential melastatin 2 (TRPM2) is a non-selective cation channel capable of permeating  $\text{Ca}^{2+}$  and is expressed in various tissues, including the brain, spleen, bone marrow, and pancreas. In particular, previous research has shown that TRPM2 knockout mice displayed impaired insulin secretion and hyperglycemia<sup>16</sup>. In addition, researchers have reported that ghrelin acts through the  $\text{G}\alpha_{12}$  signaling pathway, leading to a reduction in cyclic adenosine monophosphate (cAMP) accumulation and intracellular  $\text{Ca}^{2+}$ , and subsequent inhibition of GSIS by directly combining with GHS-R1a in  $\beta$ -cells. Nevertheless, ghrelin failed to reduce GSIS in TRPM2-KO islets, implying that the suppressive effect of ghrelin on TRPM2 channel conductance plays a crucial role in its ability to inhibit insulin secretion<sup>17</sup>.

Based on the above considerations, this study aimed to investigate whether SY exerts an antidiabetic effect by regulating the GOAT/ghrelin/GHS-R1a/cAMP/TRPM2 pathway. Experiments were performed on HFD/STZ-induced T2DM mice and cellular models of HG damage to examine the effects of SY on diabetes. SY may be a promising method to intervene in T2DM therapy.

## Materials and methods

### Reagents

Safflower Yellow (S860574) (purity  $\geq 98\%$ ) was purchased from Macklin Inc. (Macklin, Shanghai, China) and dissolved in dimethyl sulfoxide (DMSO) at a concentration of 100 mM. The storage temperature for SY was  $-80^\circ\text{C}$ . Anti-GOAT antibody was purchased from Bioss (bs-13355R). Anti-ghrelin antibody (sc-517596) and anti-GHS-R1 antibody (sc-374515) were purchased from Santa Cruz Biotechnology. Anti-insulin antibody was purchased from Affinity (AF 5109). The anti-TRPM2 antibody (ab1168) was purchased from Abcam. In addition, the goat anti-rabbit IgG (H + L) HRP (S0001) and goat anti-mouse IgG (H + L) HRP (S0002) secondary antibodies were purchased from Affinity. Goat anti-rabbit IgG (H + L) Dylight 649 (BS10034) and goat anti-mouse IgG (H + L) FITC (BS50950) were purchased from Bioworld.

### Cell culture

The mouse pancreatic  $\beta$ -cell line, MIN6, was acquired from the BeNa Culture Collection (BNCC358148). The cells were cultured in the Dulbecco's Modified Eagle's Medium (DMEM) with 5.5 mM glucose or high glucose (25 mmol/L) DMEM supplemented with 10% fetal bovine serum, 100 U/ml penicillin, and 100 mg/ml streptomycin at  $37^\circ\text{C}$  with 5%  $\text{CO}_2$ .

### Molecular docking analysis

First, we sought the amino acid sequence of GOAT from the Research Collaboratory for Structural Bioinformatics (RCSB) Protein Data Bank (PDB) website, which was then optimized using SWISS-MODEL online. The 3D configuration of SY (PubChem CID:135565560) was acquired from the PubChem Compound repository

(<https://pubchem.ncbi.nlm.nih.gov>). Next, molecular docking of GOAT and SY was carried out using AutoDock Vina 1.5.6 software<sup>18</sup>. Further, the molecular dynamic simulation of GOAT and SY was performed<sup>19</sup>.

### Cell viability assay

MIN6 cells were treated with SY dissolved in DMSO for cell treatment. DMSO was used at concentrations below 0.1%. The cells ( $6 \times 10^3$  cells/well) were cultured in 96-well dishes (Corning Inc., Corning, NY) for 24 h before incubation with various concentrations (0, 5, 10, 25, 50, 75, and 100  $\mu\text{M}$ ) of SY for 24 and 48 h. Subsequently, the cells were treated with 10  $\mu\text{l}$  of CCK-8 reagent (CCK-8, Dojindo, Japan) and incubated at 37 °C for an additional 2 h. Finally, the optical density (OD) value of each well was measured at a wavelength of 450 nm using an automated plate reader (Thermo Fisher Scientific). The cell viability was calculated by multiplying the OD of the treated group by 100% of the OD of the control group.

### Enzyme-linked immunosorbent assay (ELISA)

The concentrations of insulin, acylated ghrelin, total ghrelin, and cAMP were detected using commercially available ELISA kits according to the manufacturer's instructions.

The insulin present in the culture medium was quantified using insulin ELISA kits (JYM0351Mo) obtained from Gene Beauty Biotech in Wuhan, China. In addition, the mouse serum insulin was measured using a mouse ultrasensitive insulin ELISA kit sourced from ALPCO (Salem, NH, USA). The acylated ghrelin ELISA kit (EZRGRA) and total ghrelin ELISA kit (EZRGRT) were purchased from Sigma-Aldrich (St. Louis, MO, USA). The cAMP ELISA kit (ab234585) was purchased from Abcam (Cambridge, UK).

### Glucose-stimulated insulin secretion (GSIS)

After treatment with SY, cells were preincubated for 2 h at 37 °C in Krebs–Ringer bicarbonate Hepes buffer (KRBH) containing 0.1% bovine serum albumin (BSA) and 5.5 mmol/L glucose. For GSIS experiments, the cells were incubated with either 5.5 mmol/L or 25 mmol/L glucose for 30 min. Subsequently, supernatants were then collected for insulin analysis by insulin ELISA kit (JYM0351Mo) according to the manufacturer's instructions. Subsequently, cells were lysed in RIPA buffer (Beyotime, China) to measure intracellular insulin level. Finally, insulin secretion levels were normalized to the total insulin content.

### Western blot analysis

Cultured cells were lysed using radioimmunoprecipitation (RIPA) buffer along with a protease inhibitor complex. The protein concentration was determined using a bicinchoninic acid (BCA) kit (Beyotime, Beijing, China). Equivalent amounts of proteins were separated by 10–12% sodium dodecyl sulfate–polyacrylamide gel electrophoresis (SDS–PAGE) and transferred onto polyvinylidene fluoride (PVDF) membranes (Millipore, Billerica, MA). After blocking with 5% skim milk, the bands were incubated with primary antibodies targeting GOAT (1:1000), GHS-R1 (1:1000), and TRPM2 (1:1000) at a temperature of 4 °C for an overnight duration. Subsequently, the bands were exposed to a secondary antibody (1:10,000) for a period of 2 h at room temperature. Signals were detected using the SuperSignal West Pico Chemiluminescent Substrate (Thermo Fisher Scientific).

### Cellular thermal shift assay (CETSA)

The CETSA experiment was conducted as previously described<sup>20</sup>. Briefly, the cells were incubated with a new medium overnight in a 10 cm plate. On the following day, the cells were subjected to the specified duration (12 h) of exposure to the indicated amount (50  $\mu\text{M}$ ) of SY. An equivalent amount of DMSO was added to the control group and the cells were incubated. After incubation, cells were rinsed with phosphate buffer saline (PBS) to eliminate any surplus SY or DMSO. The suspension was centrifuged at 4500 rpm at 25 °C for 5 min. The cells were then rinsed twice with PBS and diluted with PBS to obtain a concentration of 100 million cells/ml.

Subsequently, the samples were exposed to a 3-min heat shock within the designated temperature range (37–82 °C) to induce the production of melt curves, which were then rapidly cooled to 25 °C. Next, the cells were disrupted by freezing them in liquid nitrogen for 3 min using three consecutive freeze–thaw cycles. The collected proteins and cellular waste were centrifuged at 11,800g for 20 min to form solid masses. The liquid above the sediment was then transferred to a gel-loading solution. The amount of protein was determined using western blot.

### Drug affinity responsive target stability (DARTS)

MIN6 cells were lysed using RIPA lysis buffer (Beyotime, China) containing a mixture of protease and phosphatase inhibitors. Protein concentration was determined using a BCA kit (Beyotime, Beijing, China). The cell lysates were treated with either DMSO or SY (50  $\mu\text{M}$ ) and incubated at room temperature for 2 h. The lysates were subsequently separated into six parts and subjected to digestion with various concentrations of pronase E (Roche, 10165921001) at 0, 0.01%, 0.03%, 0.1%, 0.3%, and 1% for 30 min at room temperature. Digestion was halted by boiling the samples immediately after the loading buffer was added. The 5 $\times$ protein loading buffers were included and the samples were heated to 100 °C for 5 min. Next, the samples were subjected to gel separation using SDS–PAGE.

### Immunofluorescence

MIN6 cells were cultured in 24-well plates for 24 h. Subsequently, cells were rinsed with cold PBS and fixed with 4% paraformaldehyde at 4 °C for 15 min. The cells were permeabilized using 0.1% Triton X-100 for 15 min and blocked with 5% BSA for 1 h. After three additional washes with PBS, primary antibodies targeting GOAT (1:200), ghrelin (1:100), and insulin (1:100) were added and the cells were incubated overnight at 4 °C. After three additional rinses with PBS, cells were incubated with a secondary antibody (1:500) for 1 h at ambient

temperature. Finally, the cells were treated with 4,6-diamino-2-phenyl indole (DAPI) and left to stand for an additional 15 min. Images were obtained using a microscope (Nikon, Japan). The fluorescence intensity was quantified using Image J software on immunofluorescence images.

### Experimental animals

C57/BL6 male mice, weighing  $20 \pm 2$  g and aged 6–8 weeks, were acquired from Changsheng Biotechnology (Liaoning, China). The mice were kept in a controlled environment with a constant temperature of 20–22 °C, humidity of 55–65%, and a constant 12/12 h light/dark cycle. Mice were reared on an adequate supply of pure water and chow. Animal experiments were conducted in accordance with the approved experimental protocols and standards established by the Animal Ethics Committee of the First Hospital of Jilin University (No. 2014-066), and were carried out in compliance with the ARRIVE guidelines.

After 1 week of adaptation, the animals were arbitrarily separated into two groups: the standard control group (control,  $n=8$ ) was fed ordinary feed, and the HFD group ( $n=32$ ) was fed a high-fat diet (31.1% fat, 53.3% carbohydrate, and 15.6% protein). After 6 weeks of HFD consumption, the mice were administered intraperitoneal injections of streptozotocin (STZ) at a dose of 50 mg/kg/day, which was dissolved in freshly prepared 0.1 M citrate buffer, for five consecutive days. Before STZ administration, mice fasted overnight. After a period of 72 h following the last STZ injection, mice exhibiting fasting blood glucose (FBG) levels exceeding 16.7 mmol/L were categorized as having diabetes. These diabetic mice were subsequently housed in groups of four ( $n=6-8$ ) in a random manner and were fed an HFD until the conclusion of the research.

### Experimental design and drug treatments

The mice were categorized into the following groups: (a) control group, (b) STZ+HFD (model group), (c) STZ+HFD+50 mg/kg SY (low-dose SY group), (d) STZ+HFD+100 mg/kg SY (medium-dose SY group), and STZ+HFD+200 mg/kg SY (high-dose SY group). SY was dissolved in a saline solution of 0.1 mg/ml and administered daily via intraperitoneal injection for 8 weeks. Saline solution was administered to the control and model groups. Glucose and insulin tolerances were assessed after 8 weeks. Carbon dioxide anesthesia was used to euthanize the mice after the experiments.

### Health status assessment of mice

The health of the mice was evaluated using a body condition scoring (BCS) system and an activity scoring (AS) system<sup>21,22</sup>. Trained observers conducted the assessment in the designated animal holding room. The BCS procedure adhered to established protocols and encompassed a scale ranging from 1 to 5. A score of 3 was considered the baseline or well-condition. A score of 4 indicated an overconditioned and adipose mouse, while a score of 5 denoted obesity. Conversely, a score of 2 represented an underconditioned mouse exhibiting signs of muscular wasting, and a score of 1 indicated an emaciated mouse with severe muscular wasting. In addition to evaluating the general well-being of the mice, the activity score was determined by assessing their level of movement within the cage and their gait, as previously outlined<sup>23,24</sup>. A score of 0 denoted normal activity, indicating that the mice were alert and responsive. A score of 1 indicated a slight reduction in activity or a mild deviation from the typical gait. A score of 2 indicated significantly impaired movement or a pronounced alteration in gait. Lastly, a score of 3 indicated a reluctance to move or a complete absence of movement.

### Oral glucose tolerance test (OGTT) and insulin tolerance test (ITT)

After an 8-week SY administration, the animals underwent an OGTT using a slightly modified procedure<sup>25</sup>. In summary, after 12-h fasting period, all animals were given 2.0 g/kg of glucose orally. Blood was extracted from the tail tip at intervals of 0, 30, 60, 90, and 120 min to measure the levels of glucose in the serum. A glucometer (Yuyue, 580, China) was used to measure glucose concentration.

The ITT was conducted three days after the OGTT. Briefly, after overnight fasting, the mice received a subcutaneous injection of 0.75 U/kg of insulin. Blood glucose levels were measured 0, 30, 60, 90, and 120 min after insulin administration. The area under the curve (AUC) of OGTT and ITT was calculated using the trapezoidal rule.

After completion of the experiment, the mice underwent 12 h of fasting before being euthanized. Serum was obtained by collecting blood and subjecting it to centrifugation at 3500 rpm (4 °C) for 20 min. Further analyses required the tissues to be stored at  $-80$  °C.

### Hematoxylin–eosin (H&E) and immunohistochemical (IHC) staining

Mouse pancreatic tissues were immersed in a 4% solution of polyformaldehyde for 48 h. After this, the tissues were dehydrated through the sequential application of ethanol solutions and subsequently embedded in paraffin. Subsequently, the paraffin blocks underwent a cooling and hardening process, followed by slicing into sections with a thickness of 5  $\mu$ m. After wax removal and dehydration, the sections were stained with hematoxylin and eosin (H&E) to facilitate morphological examination. Furthermore, additional sections were subjected to incubation with primary antibodies targeting insulin (1:100), GOAT (1:200), and ghrelin (1:50) at a temperature of 4 °C for an overnight duration. Subsequently, the sections were exposed to a secondary antibody for a period of 2 h at room temperature. Ultimately, the sections were stained using diaminobenzidine (DAB) and counterstained with hematoxylin. Histopathological analysis was conducted by observing the stained tissues using an optical microscope (Olympus BX60, Japan), and images were captured.

The scoring and histological analysis were conducted in a double-blind manner by two impartial observers. The mean number of islets was determined by counting them in three distinct microscopic fields, and the average number per field was calculated for each experimental group. The assessment of islet size involved measuring the maximum diameter of the islets. The islets were assessed in three separate microscopic fields, and the average



size of the islets in each group of rats was calculated<sup>26</sup>. The  $\beta$ -cell mass was calculated by insulin-positive area/total pancreas area multiplied by pancreas weight. In addition, the assessment of endocrine pancreatic injury involved the analysis of various aspects of the islets, including their architecture, inflammatory infiltrate, fibrosis, vacuolization, and intra-islet congestion<sup>27</sup>. Each slide was subjected to a semi-quantitative rating system, wherein a score ranging from 0 (indicating minimal damage) to 3 (indicating severe and extensive damage) was assigned. The extent of damage was categorized as 0 (absent), 1 (mild), 2 (moderate), or 3 (severe). The final score for each sample was determined by calculating the average of the scores observed in islets. Furthermore, the process of immunohistochemical quantification was conducted using the ImageJ software on 10 distinct fields of a section. Results are presented as a mean count of positive cells percentage of islet area.

### Statistical analysis

Statistical analysis was conducted using the GraphPad Prism version 9 (GraphPad Software, USA). The normal distribution assumption for statistical tests was confirmed by the Shapiro–Wilk test. For normally distributed data, comparisons were made using one-way analysis of variance (ANOVA) with either Dunnett's test or Tukey's test. For nonnormally distributed data, comparisons were made using Mann–Whitney U test or Kruskal–Wallis test. Data are presented as the mean  $\pm$  standard (SD) error and a *P* value  $< 0.05$  denoted a significant statistical difference.

## Results

### Molecular docking analysis reveals SY directly targeted GOAT

In this study, molecular docking was performed to explore the potential binding mode of GOAT to SY. Figure 1A,C show the binding mode of GOAT with SY. Hydrogen bonding and hydrophobic interactions were observed in the binding of GOAT and SY. As shown in Fig. 1B,D, SY formed hydrogen bonds with His, Tyr, Arg, Thr, Leu, Glu of the receptor GOAT protein at the binding pocket. In addition, the molecular dynamic simulations were conducted to show lifetime of the contacts (Fig. 1E,F). The findings from these experiments clearly indicated that SY specifically targeted GOAT.

### SY cytotoxicity in MIN6 cells

To assess the toxic effects of SY, MIN6 cells were treated with increasing concentrations of SY (0–100  $\mu$ M) for 24 and 48 h. The impact on cell growth was examined using the CCK-8 assay. As shown in Fig. 2A, SY did not exhibit any toxic effects on MIN6 cells for 24 h at concentrations up to 100  $\mu$ M. Meanwhile, after 48 h of incubation, cell proliferation started to decline in a dose-dependent manner, ranging from 10 to 100  $\mu$ M; however, these findings did not reach statistical significance ( $P > 0.05$ ).

### Effects of SY on GOAT and ghrelin expression in MIN6 cells

To examine whether SY blocks GOAT and ghrelin production in mice, we explored the direct effects of SY on GOAT and ghrelin synthesis and secretion in MIN6 cells. As illustrated in Fig. 2B–F, GOAT was detected in the MIN6 cells. SY decreased GOAT protein levels in a concentration-dependent manner in MIN6 cells after 24 h, with the most obvious inhibitory effect at 50  $\mu$ M (Fig. 2B,E). The EC<sub>50</sub> of SY was 13.74  $\mu$ M (Fig. 2D). Subsequently, we found that 50  $\mu$ M SY decreased GOAT protein levels in MIN6 cells in a time-dependent manner (Fig. 2C,F). Moreover, significant inhibition of GOAT occurred as early as 6 h and lasted up to 24 h.

We then examined insulin secretion in the cell culture medium and found that MIN6 cells secreted the maximum amount of insulin when treated with an SY concentration of 50  $\mu$ M for 12 h (Fig. 2J,N). As shown in Fig. 2G,I, in MIN6 cells, SY markedly inhibited the medium content of acyl ghrelin in a concentration-dependent manner, with the maximum inhibition observed at 12 h after administration (Fig. 2K,M). Nevertheless, the serum levels of total ghrelin did not show any notable effects (Fig. 2H,L). Based on these results, we treated the cells with 50  $\mu$ M concentration of SY for 12 h for subsequent experiments.

### SY is directly linked to GOAT and suppresses GTPase function

To verify the direct interaction between SY and GOAT proteins, two traditional methods, CETSA and DARTS, were used to detect the drug binding to the target protein. The stability of proteins can be altered by the binding of ligands, which is utilized by various techniques to evaluate target engagement. These techniques include reduced proteolytic digestion and resistance to thermally induced denaturation<sup>28,29</sup>. The CETSA results demonstrated that SY treatment effectively shielded the GOAT protein from degradation as the temperature increased, in contrast with the control group. As illustrated in Fig. 3A–D, in the vehicle-treated cell lysate, GOAT began to deteriorate at 47 °C and nearly vanished at 72 °C, whereas in the SY-treated cell lysate, GOAT degraded at 57 °C and completely disappeared at 82 °C.

We also used the DARTS assay to verify the direct interaction between SY and GOAT proteins (Fig. 3E,F). After a 12-h exposure to 50  $\mu$ M SY, WB analysis of the DARTS sample revealed a notable enhancement in the stabilization of GOAT protein levels. This enhancement was observed when various concentrations of pronase E (0, 0.01%, 0.03%, 0.1%, 0.3%, and 1%) were introduced to the entire protein extract. These findings suggest that SY can enhance the resistance of GOAT to protease E. Together, these data from CETSA and DARTS suggested that SY is directly linked to GOAT and suppressed its GTPase function in MIN6 cells.

### SY inhibits ghrelin secretion and promotes HG-induced insulin secretion in MIN6 cells

We further observed the effects of SY on ghrelin and cellular insulin secretion in the presence of high glucose levels in Min6 cells. First, we determined ghrelin and total ghrelin levels in the medium using ELISA. As shown in Fig. 4A,B, acyl ghrelin, rather than total ghrelin, was reduced in HG-induced MIN6 cells compared with that in the control group, whereas treatment with SY further reduced ghrelin levels. Next, we investigated the effects

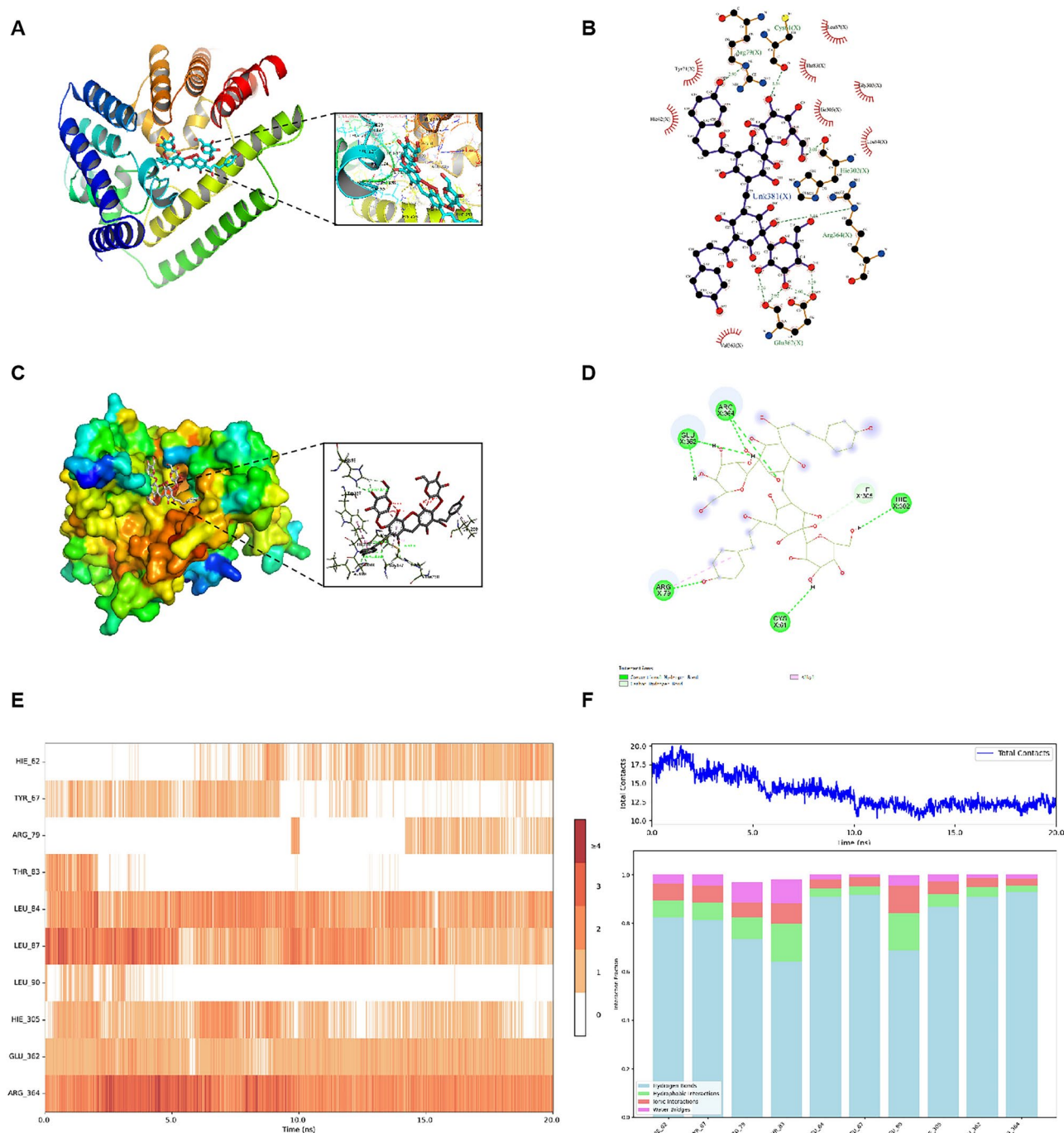


**Fig. 1.** Protein–ligand contact analysis between SY and GOAT. (A,C) 3D interaction diagram. (B,D) 2D interaction diagram. (E,F) Timeline and bar chart presentation.

of SY on GSIS in MIN6 cells using ELISA. SY significantly promoted GSIS in the presence of 25 mM glucose (Fig. 4C). Thus, SY inhibited ghrelin secretion and promoted HG-induced insulin secretion in MIN6 cells.

#### Expression and co-localization of GOAT, ghrelin and insulin in MIN6 cells

To analyze the positional relationship between GOAT, ghrelin, and insulin in MIN6 cells and the effects of HG and SY treatment on this relationship, we analyzed the expression and co-localization of GOAT, ghrelin and insulin by immunofluorescence. Results demonstrated that GOAT (red) can be co-located with ghrelin (green) signals, the numbers of GOAT (red) and ghrelin (green) signals were reduced after treatment with HG, whereas the reduction was more pronounced when combined with SY (Fig. 4D). Furthermore, the co-localization of insulin (red) with ghrelin (green) in MIN6 cells is demonstrated in Fig. 4E. It is noteworthy that the fluorescence intensity of insulin exhibited an increase following treatment with HG, and the administration of SY further

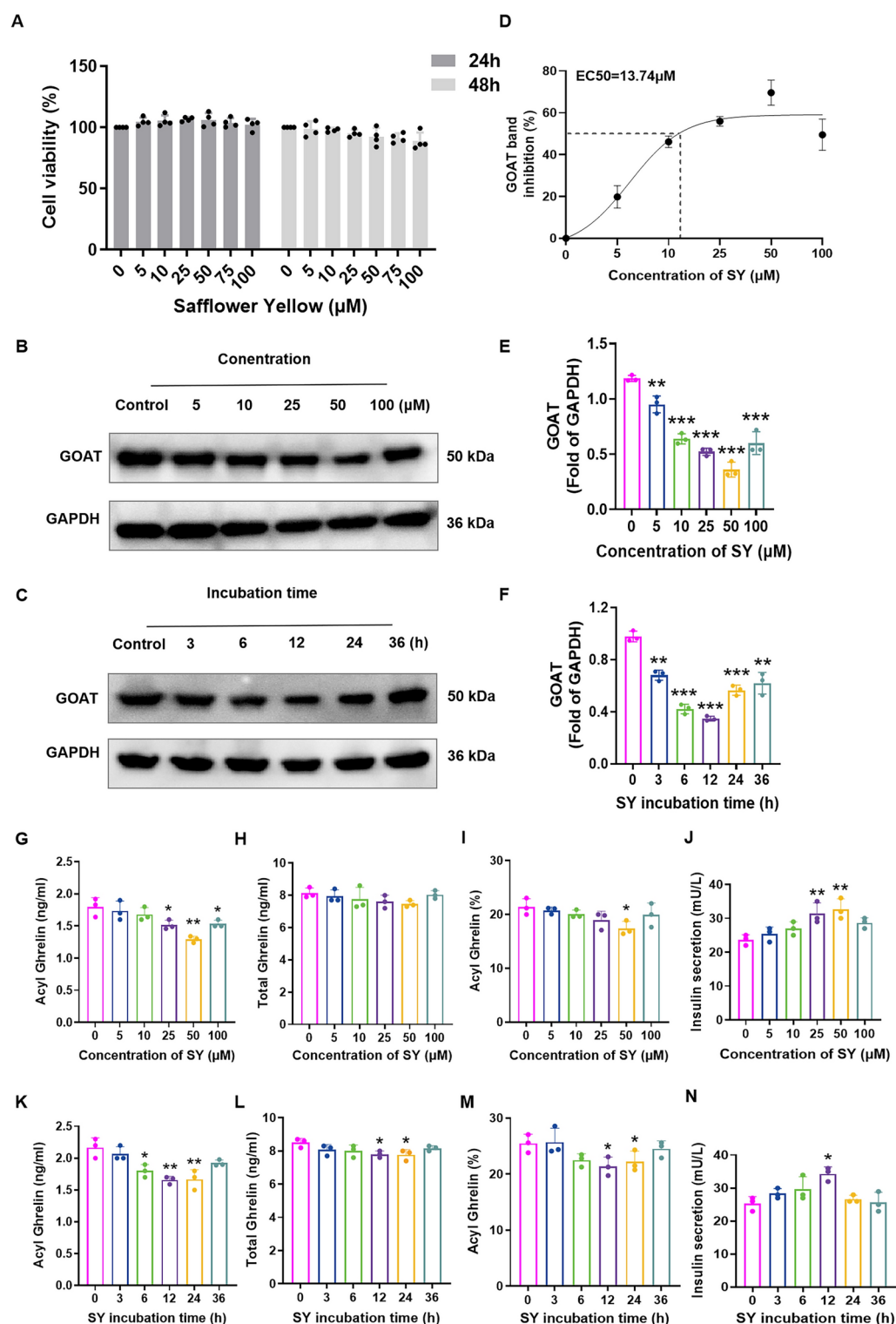


**Fig. 2.** Inhibition of GOAT and ghrelin synthesis and secretion by SY in MIN6 cells. **(A)** SY doesn't induces cytotoxicity in MIN6 cells. Cultured MIN6 cells were treated with **(B,E,G–J)** various concentrations of SY (0–100  $\mu$ M) for 24 h, or **(C,F,K–N)** SY (50  $\mu$ M) for the time indicated. **(B,C,E,F)** Representative western blots of GOAT and GAPDH. **(D)** Dose response curve of the GOAT response against SY. The percentage of GOAT inhibition was calculated by **(B)** and **(E)**. EC<sub>50</sub>, half-maximum effective concentration. **(J,N)** Medium insulin levels were determined using enzyme immunoassay. **(G,H,K,L)** Acyl-ghrelin and total ghrelin levels in the medium were determined. **(I,M)** Acyl-ghrelin levels as a percentage of total ghrelin. All experiments were repeated three times independently. Statistical significance was determined by ANOVA with Dunnett's test **(A,E–M)** or Kruskal–Wallis test **(N)**. Results are expressed as the mean  $\pm$  SD and \* $P$  < 0.05, \*\* $P$  < 0.01, \*\*\* $P$  < 0.001 versus control group.

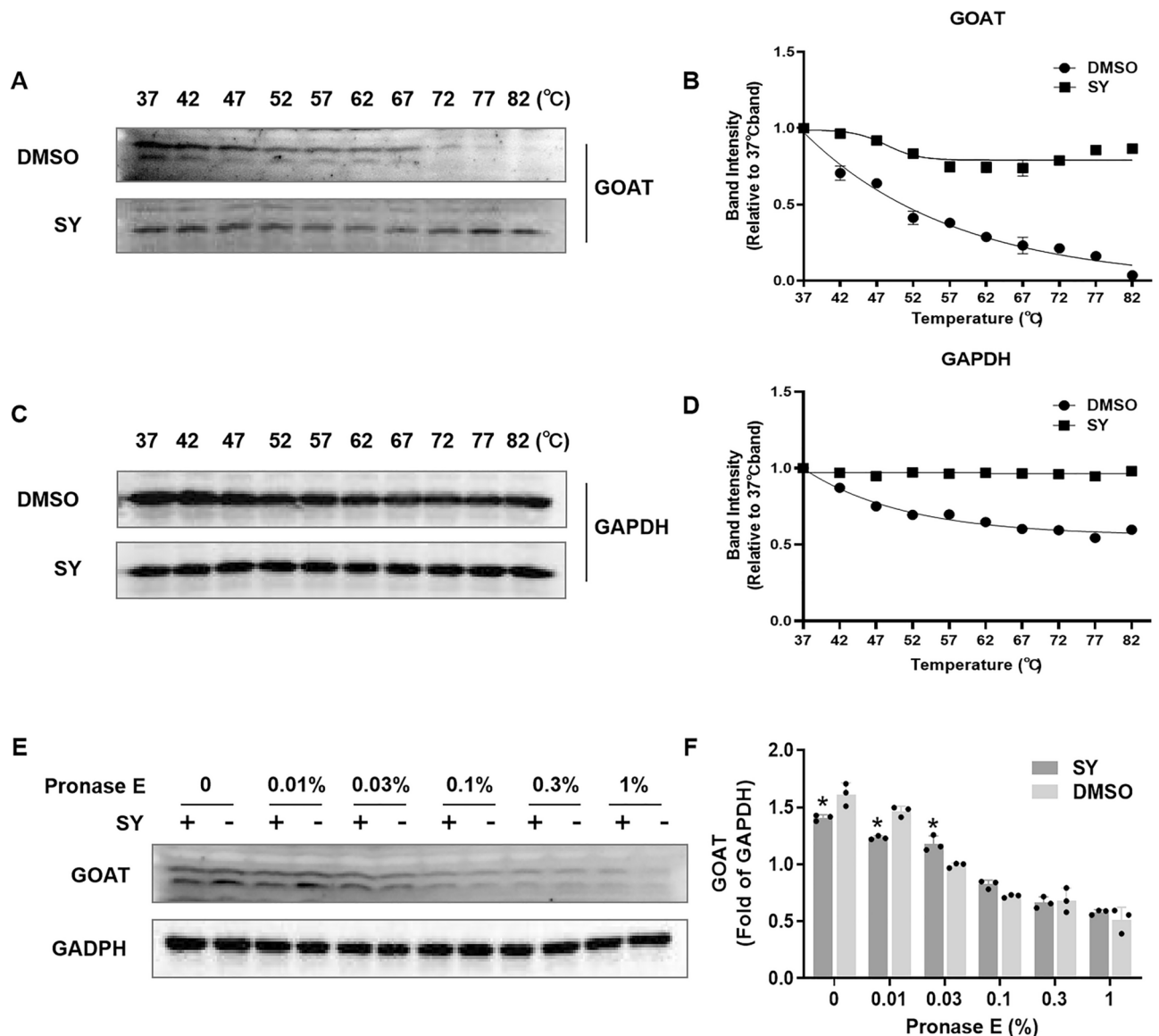


**Fig. 3.** (A,C) Lysates from MIN6 cells were incubated with or without SY (50 μM) for 12 h and subjected to CETSA assay. SY protects the target protein against temperature-dependent degeneration in MIN6 cells. GOAT was normalized with GAPDH. Note that the membrane was cropped to remove irrelevant parts. (B,D) The depiction of CETSA after quantification using western blot. (E) Lysates from MIN6 cells were incubated with or without SY (50 μM) for 12 h. Different concentrations of pronase E (0, 0.01%, 0.03%, 0.1%, 0.3%, and 1%) were added for 30 min, and GOAT content was detected using western blot analysis. Note that the membrane was cropped to remove irrelevant parts. SY promoted the resistance of the target protein GOAT to proteases. (F) The depiction of DARTS after quantification using western blot analysis. All experiments were repeated three times independently. Statistical significance was determined by ANOVA with Dunnett's test (B,D,F). Results are expressed as the mean ± SD, and \* $P < 0.05$  versus control group.

augmented insulin secretion. These data suggested that GOAT and insulin co-locates with ghrelin and also verified former results that SY suppressed GOAT and ghrelin expression and promote insulin secretion in MIN6 cells (Fig. 4F–H).

#### SY promotes insulin expression and secretion in HG-induced MIN6 cells by regulating the GOAT/ghrelin/GHS-R1a/cAMP/TRPM2 signaling pathway

Because SY administration reduced GOAT and ghrelin expression and increased insulin expression in MIN6 cell in vitro, we explored whether SY played these roles through the GOAT/ghrelin/GHS-R1a/cAMP/TRPM2 pathway. Based on western blot assays, GOAT and GHS-R1a were downregulated by HG stimulation in MIN6 cells, and this effect was significantly increased by SY (Fig. 5A,C). Additionally, our data exhibited that SY treatment increased HG-stimulated cAMP detected by ELISA and TRPM2 expression (Fig. 5A–C), this is consistent with previously reported ghrelin activation of GHS-R1a and modulation of cAMP/TRPM2 signaling



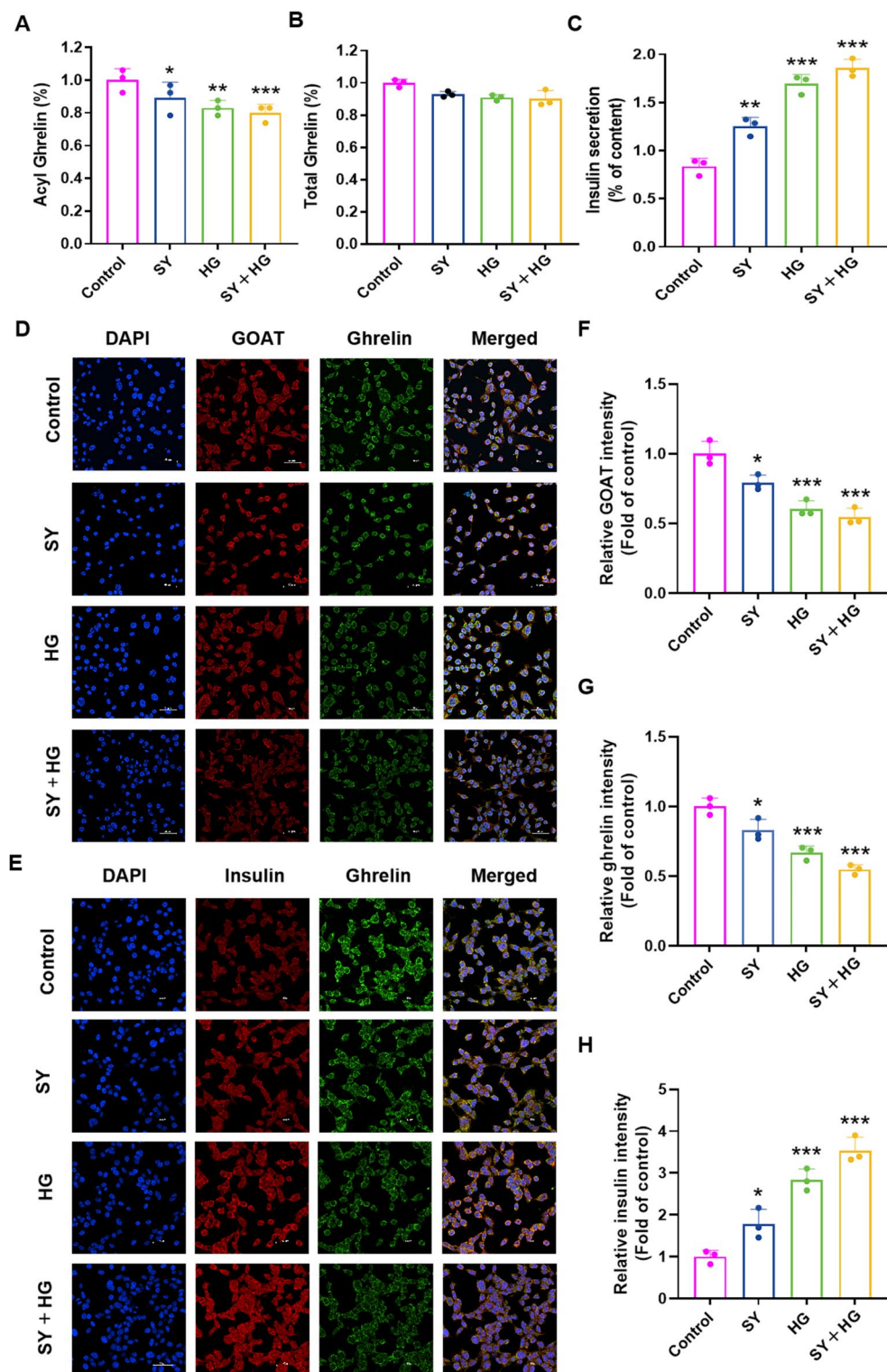


**Fig. 4.** (A,B) Effects of SY on acyl-ghrelin and total ghrelin levels in HG-induced MIN6 cells. Results are normalized to respective hormone content of control group. (C) Effects of safflower yellow (SY) on insulin secretion in HG-induced MIN6 cells. Results are normalized to the total insulin content. (D) Expression and co-localization of GOAT and ghrelin in MIN6 cells. Representative images of GOAT (red) and ghrelin (green). (E) Expression and co-localization of insulin and ghrelin in MIN6 cells. Representative images of insulin (red) and ghrelin (green). DAPI (blue) was used to stain the cell nuclei. The scale bar represents 50  $\mu$ m. (F–H) Group quantification of fluorescence intensity in (D,E). All experiments were repeated three times independently. Statistical significance was determined by ANOVA with Dunnett's test (A–C,F–H). Results are expressed as the mean  $\pm$  SD, and \* $P$  < 0.05, \*\* $P$  < 0.01, \*\*\* $P$  < 0.001 versus control group.



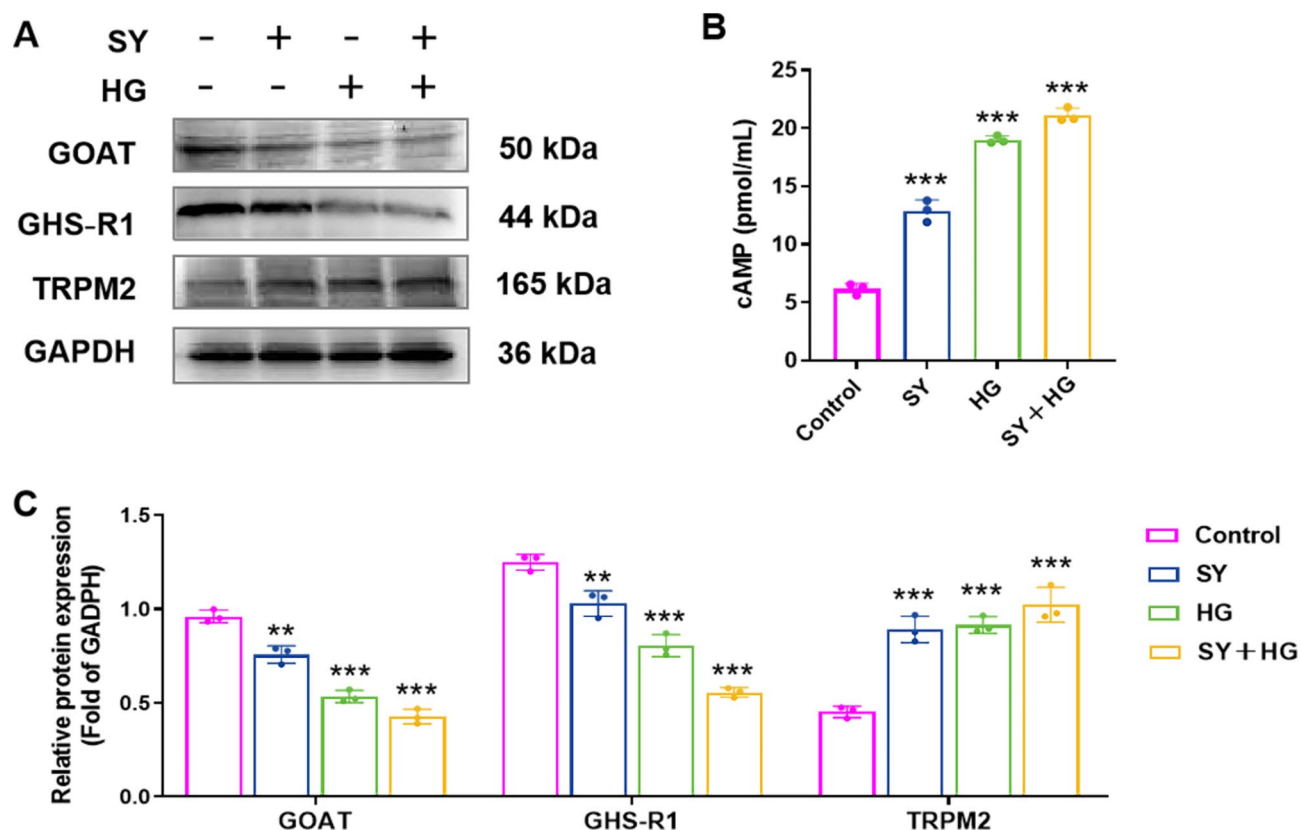


**Fig. 5.** Effects of SY on the GOAT-activated signaling pathway in HG-induced MIN6 cells. MIN6 cells were stimulated with or without SY (50  $\mu$ M) for 12 h. **(A)** Protein levels in the GOAT signaling pathway. Note that the membrane was cropped to remove irrelevant parts. **(B)** cAMP levels in the medium were determined. **(C)** Quantitative analysis of the pathway proteins. All experiments were repeated three times independently. Statistical significance was determined by ANOVA with Dunnett's test (**B,C**). Results are expressed as mean  $\pm$  SD, and \*\* $P$  < 0.01, \*\*\* $P$  < 0.001 versus control group.

to attenuate glucose-induced insulin release<sup>17</sup>. Thus, SY improved the inhibitory effect of ghrelin on cAMP and TRPM2 by inhibiting the GOAT/ghrelin/GHS-R1a signaling pathway.

### Effect of SY treatment on metabolic parameters in T2DM mice

Based on the *in vitro* experimental results that SY improves insulin secretion induced by high glucose, we investigated the effect of SY on glucose metabolism *in vivo*. First, we established a T2DM model by treating mice with HFD for six weeks and simultaneously injecting five consecutive low-dose STZ (50 mg/kg body weight). A schematic representation of T2DM induction is shown in Fig. 6A. As shown in Fig. 6B,E, the mice in the HFD + STZ group exhibited significantly higher fasting blood glucose (FBG) levels ( $P$  < 0.01) and a notable increase in body weight ( $P$  < 0.05) compared with the control group, suggesting the presence of diabetes. However, these changes were reversed when treated with SY, indicating that SY had a hypoglycemic effect. The results are described in detail below.

Weekly weight assessments of the experimental animals were performed and the results are shown in Fig. 6B. The mice in the T2DM group experienced a significant and rapid decrease in body weight, in contrast to the control group, where the weight steadily increased. However, SY hindered this reduction in body weight to some degree. The mice in the SY (100 mg/kg) group exhibited significantly greater body weight than those in the T2DM group ( $P$  < 0.05), suggesting a stronger impact of this dosage in preventing weight loss in diabetic mice. After the trial, the mice in the three different groups had greater body weights than those in the T2DM group; however, there was no notable difference observed in the SY (200 mg/kg) group ( $P$  > 0.05). We suspect the possible reason is that SY demonstrates its maximum efficacy within the concentration range of 100–200 mg/kg. Therefore, concentrations equal to or greater than 200 mg/kg may be less effective. Similar findings were reported in a study conducted by Yanli *et al.*, wherein an *in vivo* experiment was conducted<sup>30</sup>. Following a 3-month administration of SY, a Morris water maze test was conducted on the experimental mice. The results indicated a significant reduction in the latency to enter the target platform in Alzheimer's disease mice treated with SY at dosages of 10 mg/kg and 30 mg/kg, compared to those treated with normal saline ( $P$  < 0.01). However, there was no significant difference observed in mice treated with SY at a dosage of 100 mg/kg ( $P$  > 0.05).

Meanwhile, the T2DM mice exhibited a significantly increased daily food intake ( $P$  < 0.05) compared to the control group (Fig. 6C). However, following an 8-week administration of SY, the heightened food intake was

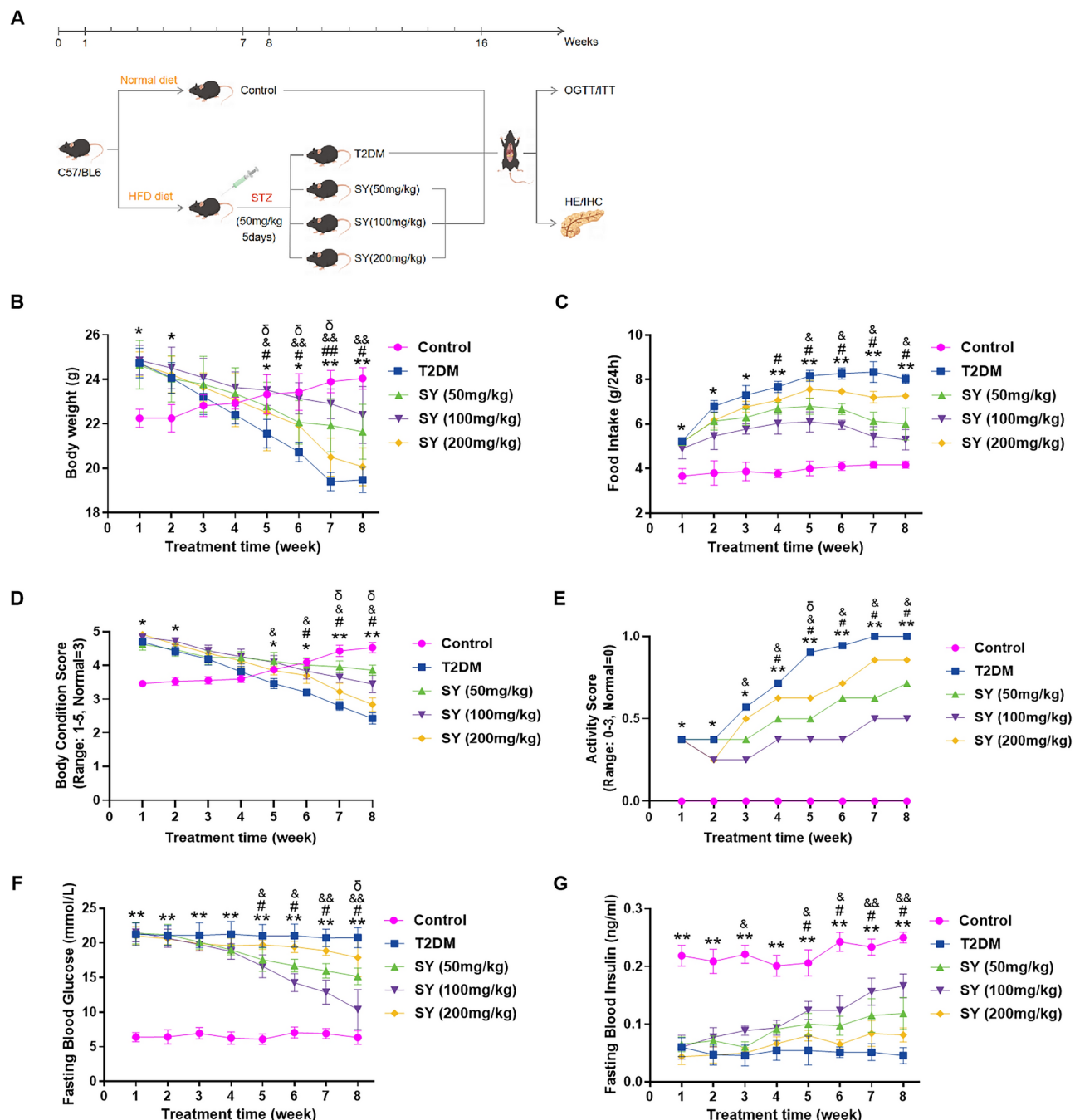


**Fig. 6.** Effects of SY on metabolic physical parameters. (A) Schematic representation of the experimental schedule. (B) Body weights of experimental mice. (C) Food intake of mice. (D) Body condition score of experimental mice. (E) Activity score of experimental mice. (F) FBG levels in experimental mice. (G) FBI levels in experimental mice. The data in (B,C,F,G) were obtained by measuring all the mice within the group (N=6–8). The experiments in (D) and (E) were repeated three times independently. Statistical significance was determined by ANOVA with Tukey's test (B,D–G) or Kruskal–Wallis test (C). Results are expressed as the mean  $\pm$  SD, and \* $P$  < 0.05, \*\* $P$  < 0.01 versus control group; # $P$  < 0.05, ## $P$  < 0.01 versus T2DM model group; & $P$  < 0.05, && $P$  < 0.01 versus SY (50 mg/kg) group;  $\delta$  $P$  < 0.05 versus SY (100 mg/kg) group.

notably diminished. Especially, interventions of SY at doses of 50 mg/kg and 100 mg/kg partially reversed the food intake ( $P$  < 0.05) in comparison to the T2DM group.

In this study, the researchers utilized the BCS and AS systems to evaluate the overall condition of the mice, as depicted in Fig. 6D,E. The T2DM mice exhibited a state of excessive weight and slightly reduced activity compared to the control group mice ( $P$  < 0.05). Following a 5-week administration of SY, a significant improvement in overweight condition was observed in both the SY (50 mg/kg) and SY (100 mg/kg) groups ( $P$  < 0.05). Notably, after 7 weeks of SY treatment, the body condition score of the T2DM mice approached

normalcy in the SY (50 mg/kg), SY (100 mg/kg), and SY (200 mg/kg) groups. Furthermore, following an eight-week treatment period, the mice in the SY (50 mg/kg) and SY (100 mg/kg) groups demonstrated a noteworthy increase in activity levels ( $P < 0.05$ ). Notably, all mice in the SY treatment groups displayed comparable health and behavioral characteristics, with no observed clinical indications of illness, except for symptoms related to diabetes throughout the duration of the study.

A graph showing the results of the weekly FBG levels is shown in Fig. 6F. The FBG levels of T2DM mice showed a significant ( $P < 0.01$ ) increase and remained consistently high throughout the experiment, indicating the presence of diabetes when compared with the control group. After 6 weeks of SY administration, there was a significant decrease in FBG levels in both the SY (50 mg/kg) and SY (100 mg/kg) groups ( $P < 0.05$ ). Specifically, after eight weeks of treatment, FBG levels decreased significantly ( $P < 0.05$ ) in the groups receiving SY (50 mg/kg), SY (100 mg/kg), and SY (200 mg/kg). It can be observed that various levels of SY demonstrated varying degrees of hypoglycemic effects, with SY (100 mg/kg) being comparatively more potent.

As shown in Fig. 6G, the weekly fasting blood insulin (FBI) levels were detected. The T2DM mice exhibited a noteworthy ( $P < 0.01$ ) reduction in FBI levels when compared to the control group. Following an eight-week intervention, the groups administered with SY (50 mg/kg) and SY (100 mg/kg) demonstrated a significant ( $P < 0.05$ ) elevation in FBI levels. Notably, different dosages of SY exhibited diverse capacities in stimulating insulin secretion, with SY (100 mg/kg) displaying comparatively greater potency.

### SY administration improves glucose and insulin tolerance in T2DM mice

To investigate the influence of SY on glucose tolerance, an OGTT was conducted eight weeks after the intraperitoneal injection of SY, and the results are shown in Fig. 7A. Throughout the experiment, the mice in the T2DM group showed significantly ( $P < 0.01$ ) elevated blood glucose levels compared with the control mice. After 30 min of glucose administration, they reached peak glucose values. Nevertheless, SY treatment delayed and repressed the increase in maximum levels. Mice treated with SY at a dose of 100 mg/kg showed reduced blood glucose levels throughout the entire test and experienced a decreased peak at 30 min. The SY administration group consistently showed a notable reduction in the  $AUC_{OGTT}$  compared with the T2DM group

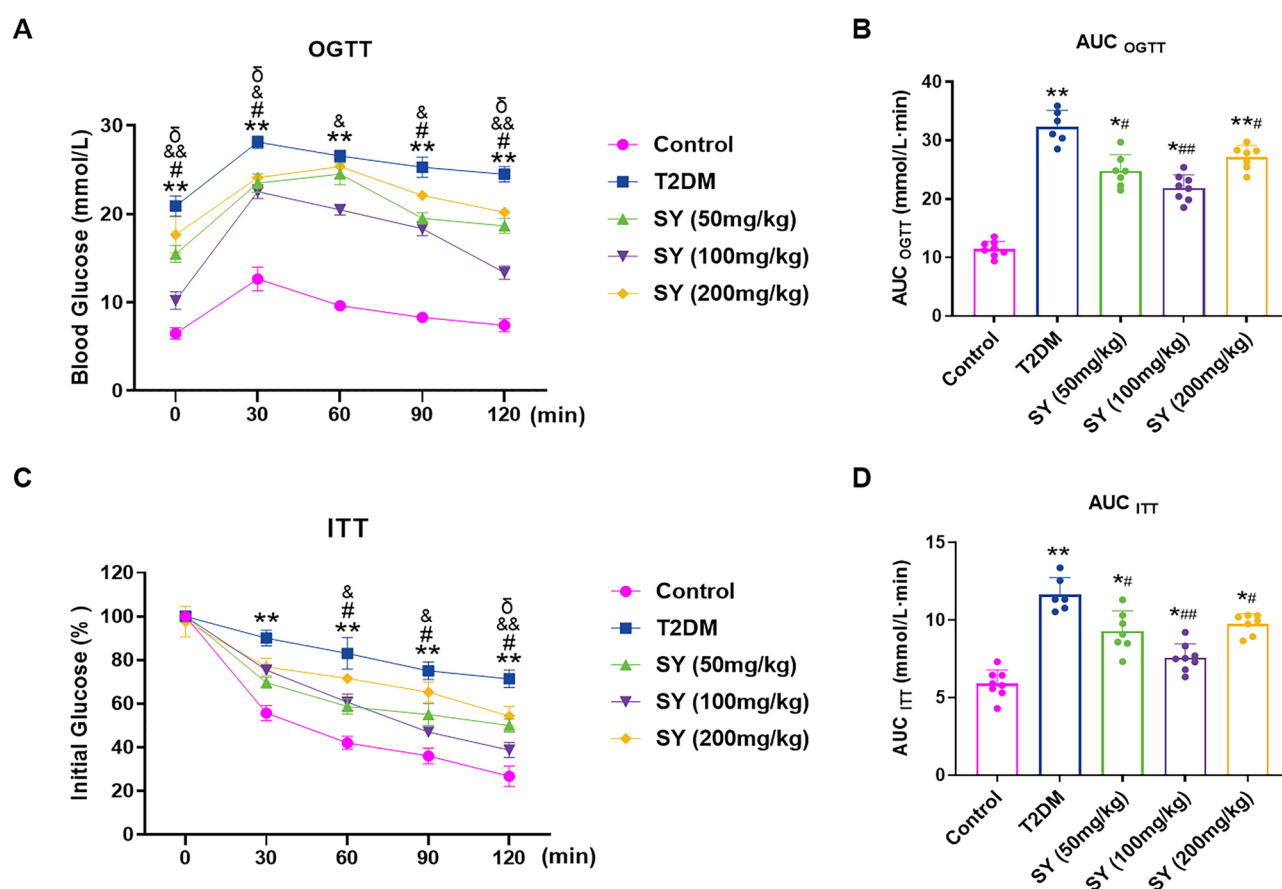


**Fig. 7.** Results of OGTT and ITT in experimental mice. (A,B) OGTT and area under the curve ( $AUC_{OGTT}$ ) were calculated and displayed. (C,D) the ITT and  $AUC_{ITT}$  were calculated and data is normalized to the percentage of initial glucose levels. The data were obtained by measuring all the mice within the group ( $N = 6-8$ ). Statistical significance was determined by ANOVA with Tukey's test. Results are expressed as the mean  $\pm$  SD, and \* $P < 0.05$ , \*\* $P < 0.01$  versus control group; # $P < 0.05$ , ## $P < 0.01$  versus T2DM model group; & $P < 0.05$ , && $P < 0.01$  versus SY (50 mg/kg) group; &# $P < 0.05$  versus SY (100 mg/kg) group.

(Fig. 7B). The OGTT is a reliable measure of how well the body responds to sudden HG levels and is frequently used to evaluate glucose processing and pancreatic  $\beta$ -cell function. In short, the findings indicated that glucose absorption and metabolism were improved in the SY (100 mg/kg) group.

Furthermore, to investigate the influence of SY on insulin resistance, ITT was performed on all experimental mice three days after the OGTT (Fig. 7C). During the ITT, the glucose levels of mice with T2DM were notably elevated compared with those of control mice at 30, 60, 90, and 120 min ( $P < 0.01$ ). In the T2DM group, the  $AUC_{ITT}$  exhibited a notable increase compared to that in the control group ( $P < 0.01$ ) (Fig. 7D). A significant reduction was observed in the SY (50 mg/kg) and SY (100 mg/kg) groups compared with that in the T2DM group ( $P < 0.05$ ), with a stronger impact observed in the SY (100 mg/kg) group than in the SY (50 mg/kg) group.  $AUC_{ITT}$  did not show any notable variation between the SY (200 mg/kg) and T2DM groups ( $P > 0.05$ ). Together, these results suggested that administration of SY at a dosage of 100 mg/kg exhibits a statistically significantly enhanced insulin sensitivity in mice with T2DM.

### SY alleviates pancreatic damage and $\beta$ -cell destruction in vivo

H&E staining was performed to observe the pancreatic morphology of mice in each group. Figure 8A shows the evaluation of the protective effect of SY on islet  $\beta$ -cell damage in T2DM mice through H&E staining of pancreatic sections. In the T2DM group, islets were irregular and shrunken, accompanied by proliferating endothelial cells and thickened capillary basement membranes. Simultaneously, a significant reduction in pancreatic islet number, islet diameter, and  $\beta$ -cells mass was observed along with steatosis and necrotic cells, suggesting impairment of the pancreatic structure by HFD/STZ (Fig. 8B–F). SY administration tends to repair pancreatic disorders by restoring the pancreatic contour and reducing vacuolation and necrosis of islet  $\beta$ -cells to different degrees. In the semi-quantitative assessment of islet tissue damage, inflammation, fibrosis, vacuolization, and intra-islet congestion were observed to be moderate to severe in the majority of rats in the T2DM group when compared to the control group (Fig. 8G–J). Treatment with varying concentrations of SY demonstrated a significant reduction in pancreatic pathological alterations to varying extents, with SY at a dosage of 100 mg/kg exhibiting the most pronounced effect.

### SY ameliorates HFD/STZ-induced T2DM via inhibiting the GOAT/ghrelin signaling pathway in vivo

To further validate the mechanism of the hypoglycemic effects of SY in vivo, we performed immunohistochemistry of the mouse pancreas using GOAT-, ghrelin-, and insulin-specific antibodies (Fig. 9A). As illustrated in Fig. 9B–D, after 8 weeks of intraperitoneal injection of SY in mice, GOAT and ghrelin protein expression was significantly reduced compared with that in T2MD mice, whereas the level of insulin protein expression was increased. In summary, our findings demonstrated that SY effectively enhanced insulin secretion by inhibiting the GOAT/ghrelin pathway, corroborating the results of the *in vitro* experiments.

## Discussion

SY, one of the primary active compounds found in *Carthamus tinctorius* L., has been shown to effectively treat diabetes and its associated complications<sup>31,32</sup>. However, possible therapeutic mechanisms of SY in DM have not been thoroughly explored. The purpose of this study was to elucidate the molecular mechanism underlying the antidiabetic effects of SY. In this study, we found that SY increased insulin secretion in MIN6 cells by regulating the GOAT/ghrelin/GHS-R1a/cAMP/TRPM2 signaling pathway. Further animal experiments showed that SY ameliorated pancreatic injury and reduced vacuolation and necrosis of islet  $\beta$ -cells in the pancreas of an HFD/STZ-induced T2DM mouse model. We also found that SY improved abnormal glucose tolerance and partially restored insulin resistance in T2DM mice. Collectively, these findings suggest that SY exerts its antidiabetic effects possibly by regulating the GOAT/ghrelin/GHS-R1a/cAMP/TRPM2 pathway (Fig. 10). Further experiments involving knocking down GOAT/ghrelin and the use of GOAT/GHSR/GHRL knockout mice are required to show an absolute requirement for these pathways.

Considering the significance of ghrelin in regulating energy metabolism and maintaining glucose balance, this study was designed to treat diabetes or obesity by regulating the ghrelin system. Ghrelin is a unique substrate for GOAT in the human proteome<sup>33</sup>. Therefore, blocking ghrelin activity by inhibiting GOAT should be the most preferred strategy, given the existence of numerous potent GOAT inhibitors that have been created in both academic and industrial settings<sup>34</sup>. Based on the above, we aimed to screen and identify a natural inhibitor of GOAT by docking with a Chinese herbal compound library, which was downloaded from the PubChem Compound database. After the preliminary experiments, we further verified the inhibitory effects of the Chinese herbal compounds on GOAT. Eventually, we discovered that SY tightly binds to GOAT and inhibits its expression in islet  $\beta$ -cells; therefore, SY was selected for further investigation. To the best of our knowledge, this is the first study to demonstrate that the active constituents of Chinese herbs can function as innate inhibitors of GOAT, thereby introducing a novel perspective for investigating the impact of GOAT on diabetes.

Identifying the target is crucial for understanding the effectiveness of the medication. Once macromolecules are targeted, traditional Chinese medicine exerts its physiological effects by regulating downstream signaling pathways and plays an important role in disease treatment<sup>35</sup>. Based on our docking results, it appears that SY has a strong and stable affinity for GOAT (Fig. 1A,C). These findings also suggest that the bonding strength of SY is influenced by hydrogen bonding and electrostatic and hydrophobic interactions, confirming the trustworthiness of the docking model (Fig. 1B,D). By binding to proteins, small-molecule ligands improve their stability and prevent protease degradation, and the thermal stability of the protein can be increased, which is commonly referred to as the principle of DARTS and CETSA<sup>28,36</sup>. Furthermore, DARTS and CETSA, which were used to verify the binding of small molecules to their target proteins, were performed to confirm whether SY was directly combined with GOAT (Fig. 3). By combining these two methods, we confirmed that GOAT is the target of SY



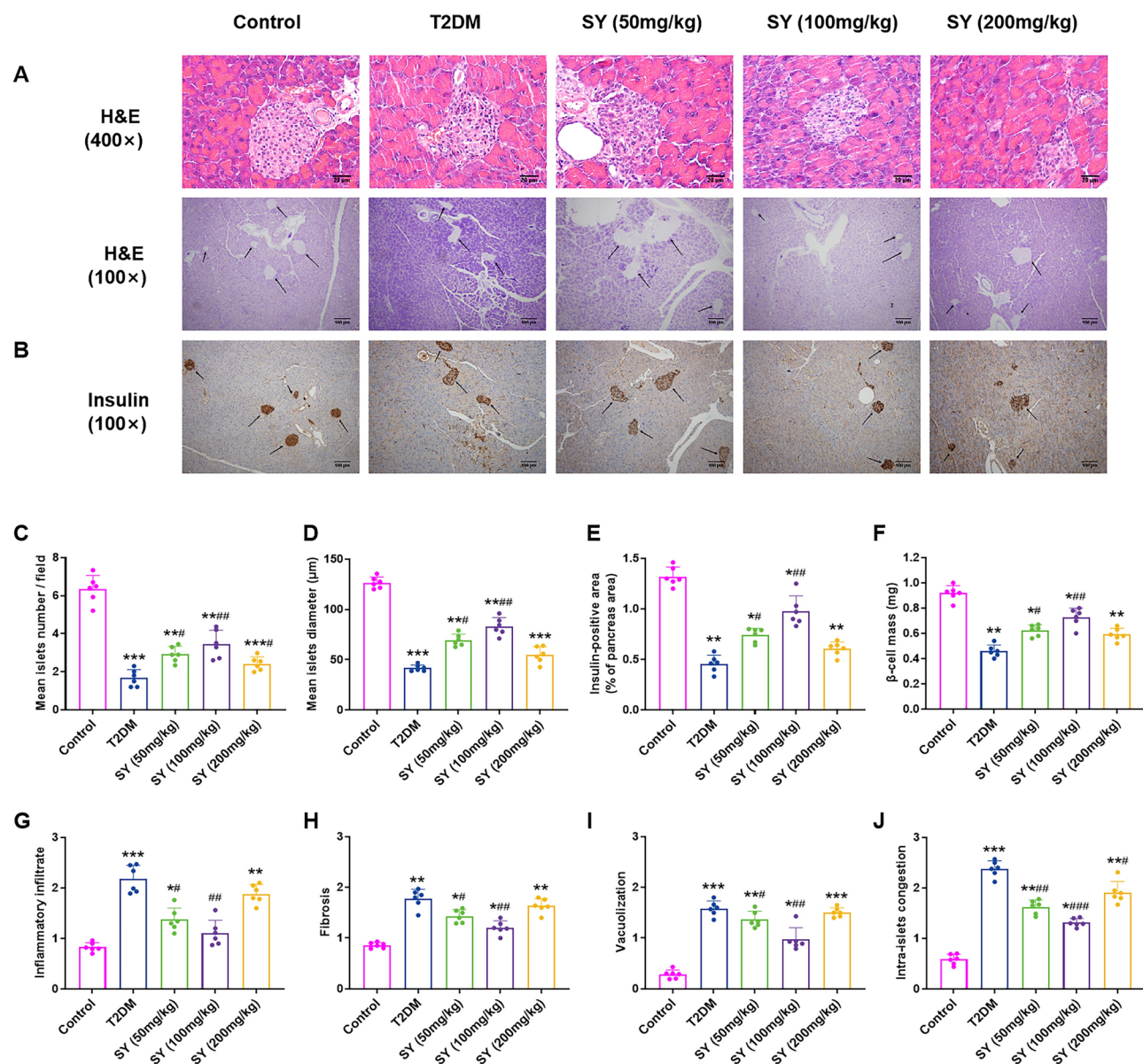


**Fig. 8.** Effect of SY on the pancreas. (A) Photomicrographs of H&E staining of pancreatic tissues. Pancreas islet sites are labeled using black arrows. The scale bar represents 200  $\mu\text{m}$  (400 $\times$ ); scale bar represents 100  $\mu\text{m}$  (100 $\times$ ). (B) Photomicrographs of IHC staining for pancreatic insulin levels. The scale bar represents 100  $\mu\text{m}$ . (C,D) The mean number and diameter of islets were determined. (E,F) quantification of insulin staining and  $\beta$ -cell mass. (G–J) Semiquantitative evaluation of inflammation infiltrate, fibrosis, vacuolization, and intra-islet congestion. Images represent two biological replicates, and 6 microscopic fields were analyzed. Statistical significance was determined by ANOVA with Tukey's test (C–H,J) or Kruskal–Wallis test (I). Results are expressed as the mean  $\pm$  SD, \* $P < 0.05$ , \*\* $P < 0.01$ , \*\*\* $P < 0.001$  versus control group; # $P < 0.05$ , ## $P < 0.01$ , ### $P < 0.001$  versus T2DM model group.

in pancreatic beta cells. Western blot analysis demonstrated that SY effectively suppressed GOAT expression in MIN6 cells. In addition, ELISA revealed that SY exhibited the ability to decrease acyl ghrelin secretion. However, no substantial variance was observed in total ghrelin levels. Collectively, these findings suggest that the suppressive effect of SY on GOAT modulates ghrelin acylation.

Furthermore, Pöykkö *et al.* demonstrated a notable reduction in fasting plasma levels of total ghrelin among individuals with T2DM. A negative association was found between ghrelin concentration, insulin levels, and insulin sensitivity<sup>37</sup>. In addition, ghrelin expression in the dorsal vagal complex neurons of rats exhibited a remarkable decrease in the hyperglycemic group, amounting to approximately 75% less than that observed in the control group<sup>38</sup>. Consistently, our findings indicate a decrease in GOAT and ghrelin expression in MIN6 cells incubated with HG and in T2DM mice compared with the control group. Currently, a substantial body of literature indicates that ghrelin exerts an inhibitory effect on glucose-stimulated insulin secretion in isolated



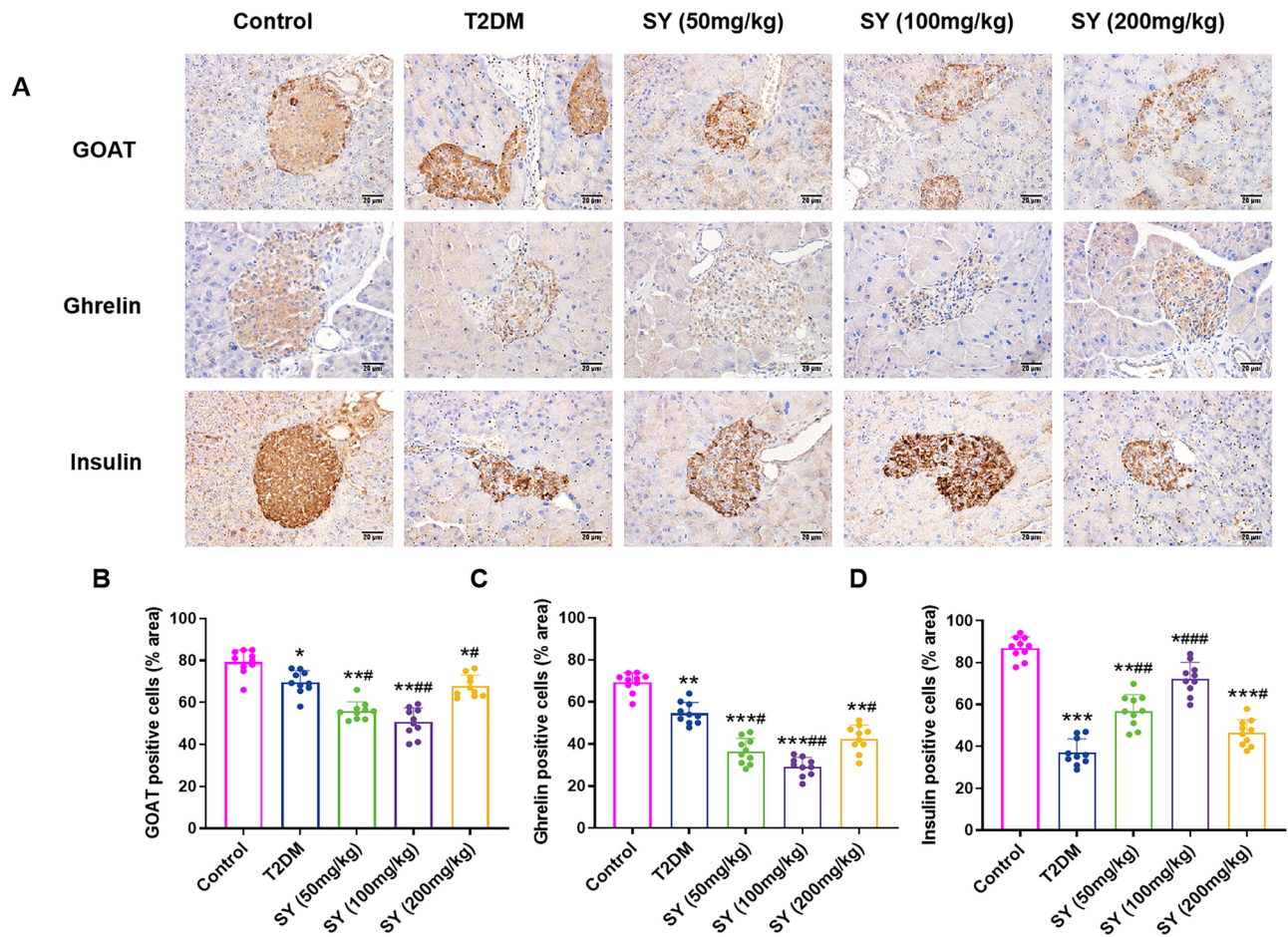


**Fig. 9.** SY ameliorates HFD/STZ-induced T2DM via inhibiting the GOAT/ghrelin signaling pathway in vivo. (A) Photomicrographs of IHC staining for pancreatic GOAT, ghrelin, and insulin levels. The scale bar represents 20  $\mu$ m. (B–D) Quantification for immunopositive cells percentage of islet area was conducted and presented in the form of bar graph. Images represent two biological replicates, and 10 microscopic fields were analyzed. Statistical significance was determined by ANOVA with Tukey's test (B–D). Results are expressed as the mean  $\pm$  SD, \* $P$  < 0.05, \*\* $P$  < 0.01, \*\*\* $P$  < 0.001 versus control group; # $P$  < 0.05, ## $P$  < 0.01, ### $P$  < 0.001 versus T2DM model group.

islets and pancreatic  $\beta$ -cells<sup>39,40</sup>. Conversely, some studies have reported a stimulatory effect of ghrelin on insulin secretion<sup>41,42</sup>. These findings suggest that the impact of ghrelin on insulin secretion is contingent upon variables such as the specific cell type employed, the concentration of ghrelin, and other experimental conditions. Consequently, discrepancies in the literature may be attributed to variations in these factors.

Notably, prior to conducting animal experiments, an extensive review of literature was undertaken to ascertain the appropriate dosage, administration method, and timing. Yanli Hu *et al.* discovered that administering SY treatment (at doses of 10 mg/kg, 30 mg/kg, and 100 mg/kg) via intragastric administration over a period of 3 months resulted in significant improvement of learning and memory deficits in APP/PS1 mice<sup>30,43</sup>. Additionally, a separate study demonstrated that the administration of oral HSYA at a dosage of 200 mg/kg per day for 12 weeks in C57BL/6J mice resulted in a reduction in obesity by influencing the composition of the gut microbiota and serum metabolism<sup>5</sup>. In light of the aforementioned studies, we have consequently chosen to employ SY concentrations of 50 mg/kg/day, 100 mg/kg/day, and 200 mg/kg/day through intraperitoneal administration for a period of 8 weeks.

The precise mechanism of insulin secretion through TRPM2, potentially by regulating intracellular calcium concentration, is not clearly understood. The cAMP-dependent protein kinase (PKA) pathway serves as a prominent downstream pathway following the activation of G protein-coupled receptors. The process of phosphorylating VGCC and other ion channels has the potential to induce increases in  $[\text{Ca}^{2+}]_i$ <sup>44</sup>. The depolarization of the membrane caused by glucose is a result of the closure of the K-ATP channel and the opening of TRPM2 channels. According to Yoshida *et al.*, glucose-induced depolarization can be further enhanced by the activation of cAMP exchange proteins (EPAC) directly activated by the cAMP/EPAC/TRPM2 channel via glucose metabolism<sup>45</sup>. The results of this study indicated that SY enhanced the levels of cAMP and TRPM2 in MIN6 cells, potentially contributing to the significant role of SY in promoting insulin secretion.

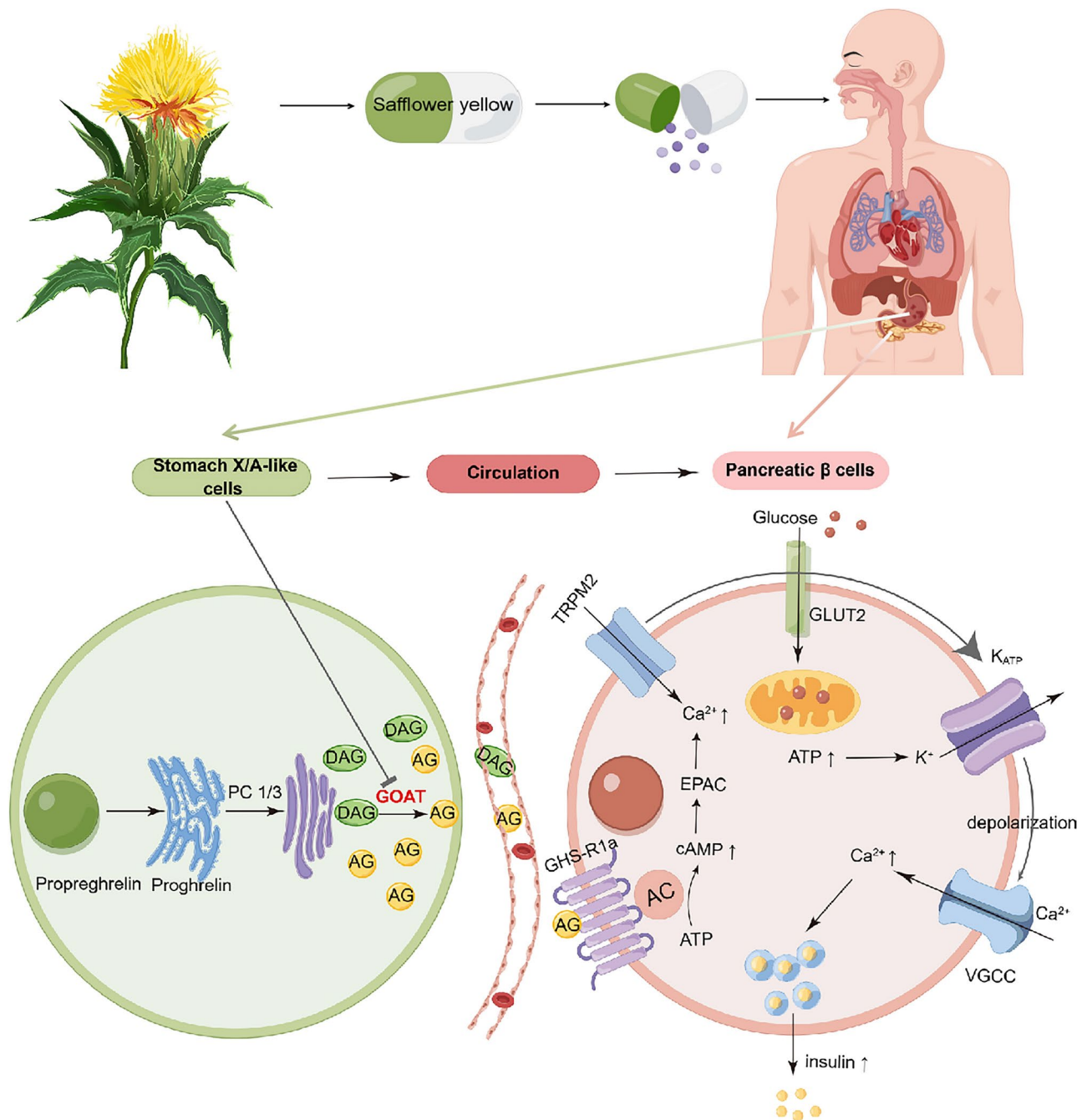


**Fig. 10.** Schematic representation of SY regulatory mechanisms. Specifically, in stomach X/A-like cells, preproghrelin undergoes cleavage to proghrelin within the endoplasmic reticulum, followed by acylation mediated by GOAT. Subsequently, proghrelin peptides undergo conversion into mature AG and DAG forms by the prohormone convertase PC1/3 and are then transported to the secretory vesicles of the Golgi apparatus. Notably, SY administration resulted in inhibition of GOAT expression, consequently leading to a decrease in AG production. Upon entering the circulatory system, AG exhibits binding affinity for GHS-R1a, thereby initiating downstream signaling. Conversely, DAG may interact with an unidentified receptor. Low AG levels may facilitate the transformation of ATP to cAMP, subsequently activating EPAC and inducing the opening of TRPM2 channels, which cooperatively facilitates depolarization and accelerates the shutting down of glucose-induced K-ATP channels. Ultimately, there is an increase in Ca<sup>2+</sup> influx and insulin secretion owing to this mechanism. SY, safflower yellow; GOAT, enzyme ghrelin O-acyltransferase; AG, acyl ghrelin; DAG, des-acyl ghrelin; GHS-R1a, growth hormone secretagogue receptor 1a; EPAC, exchange protein directly activated by cAMP; TRPM2, transient receptor potential melastatin 2.

In conclusion, these results suggest that SY has the potential to alleviate HFD/STZ-induced diabetes in mice and enhance GSIS in MIN6 cells by regulating GOAT/ghrelin/GHS-R1a/cAMP/TRPM2 pathway expression. The results of this study have great significance for the advancement of SY as a potential treatment for diabetes. Nevertheless, additional investigations are required to clarify the fundamental processes and conduct trials to assess the impact of SY on individuals with diabetes.

## Data availability

The data that support the findings of this study are available in the methods and material of this article.

Received: 12 June 2024; Accepted: 16 January 2025

Published online: 11 February 2025

## References

- Chaudhury, A. et al. Clinical review of antidiabetic drugs: implications for type 2 diabetes mellitus management. *Front. Endocrinol.* **8**, 6. <https://doi.org/10.3389/fendo.2017.00006> (2017).
- Mahdavi, A., Bagherniya, M., Mirenayat, M. S., Atkin, S. L. & Sahebkar, A. Medicinal plants and phytochemicals regulating insulin resistance and glucose homeostasis in type 2 diabetic patients: a clinical review. *Adv. Exp. Med. Biol.* **1308**, 161–183. [https://doi.org/10.1007/978-3-030-64872-5\\_13](https://doi.org/10.1007/978-3-030-64872-5_13) (2021).
- Ao, H., Feng, W. & Peng, C. Hydroxysafflor yellow A: a promising therapeutic agent for a broad spectrum of diseases. *Evid.-Based Complement. Altern. Med. eCAM* **2018**, 8259280. <https://doi.org/10.1155/2018/8259280> (2018).
- Zhu, H. et al. The mechanism by which safflower yellow decreases body fat mass and improves insulin sensitivity in HFD-induced obese mice. *Front. Pharmacol.* **7**, 127. <https://doi.org/10.3389/fphar.2016.00127> (2016).
- Liu, J. et al. Oral hydroxysafflor yellow A reduces obesity in mice by modulating the gut microbiota and serum metabolism. *Pharmacol. Res.* **134**, 40–50. <https://doi.org/10.1016/j.phrs.2018.05.012> (2018).
- Yan, K. et al. Safflower yellow and its main component HSYA alleviate diet-induced obesity in mice: possible involvement of the increased antioxidant enzymes in liver and adipose tissue. *Front. Pharmacol.* **11**, 482. <https://doi.org/10.3389/fphar.2020.00482> (2020).
- Kojima, M. et al. Ghrelin is a growth-hormone-releasing acylated peptide from stomach. *Nature* **402**, 656–660. <https://doi.org/10.1038/45230> (1999).
- Müller, T. D. et al. Ghrelin. *Mol. Metab.* **4**, 437–460. <https://doi.org/10.1016/j.molmet.2015.03.005> (2015).
- Yang, J., Brown, M. S., Liang, G., Grishin, N. V. & Goldstein, J. L. Identification of the acyltransferase that octanoylates ghrelin, an appetite-stimulating peptide hormone. *Cell* **132**, 387–396. <https://doi.org/10.1016/j.cell.2008.01.017> (2008).
- Churm, R., Davies, J. S., Stephens, J. W. & Prior, S. L. Ghrelin function in human obesity and type 2 diabetes: a concise review. *Obes. Rev.* **18**, 140–148. <https://doi.org/10.1111/obr.12474> (2017).
- Collén, G., Tschöp, M. H. & Müller, T. D. Therapeutic potential of targeting the ghrelin pathway. *Int. J. Mol. Sci.* <https://doi.org/10.3390/ijms18040798> (2017).
- Lindqvist, A. et al. Ghrelin suppresses insulin secretion in human islets and type 2 diabetes patients have diminished islet ghrelin cell number and lower plasma ghrelin levels. *Mol. Cell. Endocrinol.* **511**, 110835. <https://doi.org/10.1016/j.mce.2020.110835> (2020).
- Heppner, K. M. & Tong, J. Mechanisms in endocrinology: regulation of glucose metabolism by the ghrelin system: multiple players and multiple actions. *Eur. J. Endocrinol.* **171**, R21–32. <https://doi.org/10.1530/eje-14-0183> (2014).
- Sun, Y., Asnicar, M., Saha, P. K., Chan, L. & Smith, R. G. Ablation of ghrelin improves the diabetic but not obese phenotype of ob/ob mice. *Cell Metab.* **3**, 379–386. <https://doi.org/10.1016/j.cmet.2006.04.004> (2006).
- Zhao, T. J. et al. Ghrelin O-acyltransferase (GOAT) is essential for growth hormone-mediated survival of calorie-restricted mice. *Proc. Natl. Acad. Sci. U.S.A.* **107**, 7467–7472. <https://doi.org/10.1073/pnas.1002271107> (2010).
- Pang, B. et al. Glucagon-like peptide-1 potentiates glucose-stimulated insulin secretion via the transient receptor potential melastatin 2 channel. *Exp. Ther. Med.* **14**, 5219–5227. <https://doi.org/10.3892/etm.2017.5136> (2017).
- Kurashina, T. et al. The  $\beta$ -cell GHSR and downstream cAMP/TRPM2 signaling account for insulinostatic and glycemic effects of ghrelin. *Sci. Rep.* **5**, 14041. <https://doi.org/10.1038/srep14041> (2015).
- Trott, O. & Olson, A. J. AutoDock Vina: improving the speed and accuracy of docking with a new scoring function, efficient optimization, and multithreading. *J. Comput. Chem.* **31**, 455–461. <https://doi.org/10.1002/jcc.21334> (2010).
- H.M.A.D.A. et al. Amber 2021, (University of California, 2021).
- Jafari, R. et al. The cellular thermal shift assay for evaluating drug target interactions in cells. *Nat. Protoc.* **9**, 2100–2122. <https://doi.org/10.1038/nprot.2014.138> (2014).
- Ullman-Culleré, M. H. & Foltz, C. J. Body condition scoring: a rapid and accurate method for assessing health status in mice. *Lab. Anim. Sci.* **49**, 319–323 (1999).
- Awosanya, O. D. et al. Osteoclast-mediated bone loss observed in a COVID-19 mouse model. *Bone* **154**, 116227. <https://doi.org/10.1016/j.bone.2021.116227> (2022).
- Nunamaker, E. A., Anderson, R. J., Artwohl, J. E., Lyubimov, A. V. & Fortman, J. D. Predictive observation-based endpoint criteria for mice receiving total body irradiation. *Comp. Med.* **63**, 313–322 (2013).
- Hankenson, F. C. et al. Weight loss and reduced body temperature determine humane endpoints in a mouse model of ocular herpesvirus infection. *J. Am. Assoc. Lab. Anim. Sci.* **52**, 277–285 (2013).
- Xia, X. et al. Jiaogulan tea (*Gpostemma pentaphyllum*) potentiates the antidiabetic effect of white tea via the AMPK and PI3K pathways in C57BL/6 mice. *Food Funct.* **11**, 4339–4355. <https://doi.org/10.1039/d0fo00395f> (2020).
- Mega, C. et al. Sitagliptin prevents aggravation of endocrine and exocrine pancreatic damage in the Zucker Diabetic Fatty rat—focus on amelioration of metabolic profile and tissue cytoprotective properties. *Diabetol. Metab. Syndr.* **6**, 42. <https://doi.org/10.1186/1758-5996-6-42> (2014).
- Ferreira, L. et al. Effects of sitagliptin treatment on dysmetabolism, inflammation, and oxidative stress in an animal model of type 2 diabetes (ZDF rat). *Mediat. Inflamm.* **2010**, 592760. <https://doi.org/10.1155/2010/592760> (2010).
- Lomenick, B. et al. Target identification using drug affinity responsive target stability (DARTS). *Proc. Natl. Acad. Sci. U. S. A.* **106**, 21984–21989. <https://doi.org/10.1073/pnas.0910040106> (2009).
- Senisterra, G., Chau, I. & Vedadi, M. Thermal denaturation assays in chemical biology. *Assay Drug Dev. Technol.* **10**, 128–136. <https://doi.org/10.1089/adt.2011.0390> (2012).
- Shi, X. M. et al. Effects of safflower yellow on beta-amyloid deposition and activation of astrocytes in the brain of APP/PS1 transgenic mice. *Biomed. Pharmacother.* **98**, 553–565. <https://doi.org/10.1016/j.biopha.2017.12.099> (2018).
- Lee, M., Li, H., Zhao, H., Suo, M. & Liu, D. Effects of hydroxysafflor Yellow A on the PI3K/AKT pathway and apoptosis of pancreatic  $\beta$ -cells in type 2 diabetes mellitus rats. *Diabetes Metab. Syndr. Obes. Targets Ther.* **13**, 1097–1107. <https://doi.org/10.2147/dms.0246381> (2020).
- Lee, M. et al. Protective effect of hydroxysafflor yellow A on nephropathy by attenuating oxidative stress and inhibiting apoptosis in induced type 2 diabetes in rat. *Oxid. Med. Cell. Longev.* **2020**, 7805393. <https://doi.org/10.1155/2020/7805393> (2020).



33. Darling, J. E. et al. Structure-activity analysis of human ghrelin O-acyltransferase reveals chemical determinants of ghrelin selectivity and acyl group recognition. *Biochemistry* **54**, 1100–1110. <https://doi.org/10.1021/bi5010359> (2015).
34. Moose, J. E., Leets, K. A., Mate, N. A., Chisholm, J. D. & Hougland, J. L. An overview of ghrelin O-acyltransferase inhibitors: a literature and patent review for 2010–2019. *Expert Opin. Ther. Patents* **30**, 581–593. <https://doi.org/10.1080/13543776.2020.1776263> (2020).
35. Zeng, K. W. & Tu, P. F. Current status and challenging of direct target study of traditional Chinese medicine complex system based on solid coupling beads. *China J. Chin. Materia Medica* **42**, 3645–3649. <https://doi.org/10.19540/j.cnki.cjcm.20170907.008> (2017).
36. Chen, F. et al. Identification of adenylate kinase 5 as a protein target of ginsenosides in brain tissues using mass spectrometry-based drug affinity responsive target stability (DARTS) and cellular thermal shift assay (CETSA) techniques. *J. Agric. Food Chem.* **70**, 2741–2751. <https://doi.org/10.1021/acs.jafc.1c07819> (2022).
37. Pöykkö, S. M. et al. Low plasma ghrelin is associated with insulin resistance, hypertension, and the prevalence of type 2 diabetes. *Diabetes* **52**, 2546–2553. <https://doi.org/10.2337/diabetes.52.10.2546> (2003).
38. Huang, L. et al. Influence of fasting, insulin and glucose on ghrelin in the dorsal vagal complex in rats. *J. Endocrinol.* **211**, 257–262. <https://doi.org/10.1530/joe-11-0147> (2011).
39. Dezaki, K. et al. Endogenous ghrelin in pancreatic islets restricts insulin release by attenuating  $Ca^{2+}$  signaling in beta-cells: implication in the glycemic control in rodents. *Diabetes* **53**, 3142–3151. <https://doi.org/10.2337/diabetes.53.12.3142> (2004).
40. Wierup, N., Yang, S., McEvilly, R. J., Mulder, H. & Sundler, F. Ghrelin is expressed in a novel endocrine cell type in developing rat islets and inhibits insulin secretion from INS-1 (832/13) cells. *J. Histochem. Cytochem.* **52**, 301–310. <https://doi.org/10.1177/002215540405200301> (2004).
41. Adeghate, E. & Ponery, A. S. Ghrelin stimulates insulin secretion from the pancreas of normal and diabetic rats. *J. Neuroendocrinol.* **14**, 555–560. <https://doi.org/10.1046/j.1365-2826.2002.00811.x> (2002).
42. Date, Y. et al. Ghrelin is present in pancreatic alpha-cells of humans and rats and stimulates insulin secretion. *Diabetes* **51**, 124–129. <https://doi.org/10.2337/diabetes.51.1.124> (2002).
43. Pang, J. et al. Safflower yellow improves synaptic plasticity in APP/PS1 mice by regulating microglia activation phenotypes and BDNF/TrkB/ERK signaling pathway. *Neuromol. Med.* **22**, 341–358. <https://doi.org/10.1007/s12017-020-08591-6> (2020).
44. Leech, C. A. et al. Molecular physiology of glucagon-like peptide-1 insulin secretagogue action in pancreatic  $\beta$  cells. *Progr. Biophys. Mol. Biol.* **107**, 236–247. <https://doi.org/10.1016/j.pbiomolbio.2011.07.005> (2011).
45. Yosida, M. et al. Involvement of cAMP/EPAC/TRPM2 activation in glucose- and incretin-induced insulin secretion. *Diabetes* **63**, 3394–3403. <https://doi.org/10.2337/db13-1868> (2014).

## Acknowledgements

We are grateful to Figdraw platform ([www.figdraw.com](http://www.figdraw.com)) for drawing support. Figure 6A and 10 were drawn by Figdraw (ID: YITUYf30c4). In addition, we would like to thank KetengEdit ([www.ketengedit.com](http://www.ketengedit.com)) for its linguistic assistance during the preparation of this manuscript.

## Author contributions

W.G. and L.Y.: conceptualization, methodology. H.Z. and P.W.: supervision. Q.Y.: software. Y.M.: formal analysis, writing-original draft preparation. All authors have reviewed and approved the final manuscript.

## Funding

This work was supported by the Jilin Scientific and Technological Development Program (20220508085RC); the Jilin Scientific and Technological Development Program (YDZJ202401400ZYTS); and the Graduate Innovation Fund of Jilin University (451230411126).

## Competing interests

The authors declare no competing interests.

## Additional information

**Supplementary Information** The online version contains supplementary material available at <https://doi.org/10.1038/s41598-025-87201-6>.

**Correspondence** and requests for materials should be addressed to W.G. or L.Y.

**Reprints and permissions information** is available at [www.nature.com/reprints](http://www.nature.com/reprints).

**Publisher's note** Springer Nature remains neutral with regard to jurisdictional claims in published maps and institutional affiliations.

**Open Access** This article is licensed under a Creative Commons Attribution-NonCommercial-NoDerivatives 4.0 International License, which permits any non-commercial use, sharing, distribution and reproduction in any medium or format, as long as you give appropriate credit to the original author(s) and the source, provide a link to the Creative Commons licence, and indicate if you modified the licensed material. You do not have permission under this licence to share adapted material derived from this article or parts of it. The images or other third party material in this article are included in the article's Creative Commons licence, unless indicated otherwise in a credit line to the material. If material is not included in the article's Creative Commons licence and your intended use is not permitted by statutory regulation or exceeds the permitted use, you will need to obtain permission directly from the copyright holder. To view a copy of this licence, visit <http://creativecommons.org/licenses/by-nc-nd/4.0/>.

© The Author(s) 2025